Lab on a Chip

FRONTIER

View Article Online
View Journal

Cite this: DOI: 10.1039/c5lc00265f

Recent advances in microfluidic actuation and micro-object manipulation *via* surface acoustic waves†

Ghulam Destgeer and Hyung Jin Sung*

Received 6th March 2015,
Accepted 7th May 2015

DOI: 10.1039/c5lc00265f

www.rsc.org/loc

The realization of microscale total analysis systems and lab-on-a-chip technologies requires efficient actuation (mixing, pumping, atomizing, nebulizing, driving, *etc.*) of fluids on the microscopic scale and dexterous manipulation (separation, sorting, trapping, concentration, merging, patterning, aligning, focusing, *etc.*) of micro-objects (cells, droplets, particles, nanotubes, *etc.*) in open (sessile droplets) as well as confined spaces (microchannels/chambers). These capabilities have been recently achieved using powerful acoustofluidic techniques based on high-frequency (10–1000 MHz) surface acoustic waves (SAWs). SAW-based miniaturized microfluidic devices are best known for their non-invasive properties, low costs, and ability to manipulate micro-objects in a label-free manner. The energy-efficient SAWs are also compatible with conventional microfabrication technologies. The present work critically analyses recent reports describing the use of SAWs in microfluidic actuation and micro-object manipulation. Acoustofluidic techniques may be categorized according to the use of travelling SAWs (TSAWs) or standing SAWs (SSAWs). TSAWs are used to actuate fluids and manipulate micro-objects *via* acoustic streaming flow (ASF) as well as acoustic radiation force (ARF). SSAWs are mainly used for micro-object manipulation and are rarely employed for microfluidic actuation. We have reviewed reports of new technological developments that have not been covered in other recent reviews. In the end, we describe the future prospects of SAW-based acoustofluidic technologies.

Introduction

Efficient actuation of fluids and dexterous handling of micro-objects on the micro/nano-scale are critical to microfluidic lab-on-a-chip systems. Surface acoustic waves (SAWs) have shown remarkable potential in mixing, atomizing, or driving fluids on the micro-scale, for example, sessile droplets residing on the surfaces of a substrate (open spaces) or continuous flow inside a microfluidic channel (confined spaces).[1–4] Micro-objects, which usually include unicellular microorganisms, blood cells, cancerous (circulating tumour) cells, droplets, particles, nanotubes, *etc.*, have been effectively manipulated using SAWs.[1–4] The focus of the present review is to critically analyse and summarize the most recent work (published in year 2013 and onward) demonstrating micro-object manipulation and microfluidic actuation using SAWs. Before embarking on the main subject, we will delineate the fundamental working principles underlying SAW platforms.

An interdigitated transducer (IDT) comprising comb-shaped metal electrodes deposited on top of a piezoelectric substrate (lithium niobate, $LiNbO_3$, LN) produces surface vibrations or SAWs when actuated with an electric alternating current signal at a resonant frequency (see Fig. 1A). The SAWs that radiate away from the IDT are termed propagating or travelling SAWs (TSAWs). Two oppositely propagating TSAWs or a single TSAW reflected from a sound hard boundary constructively interferes and forms a standing SAW (SSAW). A SAW-based acoustofluidic system is composed of an acoustic wave production module (IDT) and a fluid domain with or without suspended micro-objects (see Fig. 1A). A fluid domain can be a sessile droplet, a microchannel, or a chamber.

A high-frequency acoustic wave propagating through a liquid loses its energy through viscous damping of the wave, induces acoustic streaming flow (ASF) in the fluid, and imparts an acoustic radiation force (ARF) to suspended polystyrene (PS) particles (see Fig. 1B, C). The PS particles influenced by the TSAW-based ASF or ARF may be distinguished based on the value of a κ-factor, $\kappa = \pi d/\lambda_f$, which depends on the particle diameter (d) and sound wavelength in the fluid ($\lambda_f = c_f/f$), such that f is the acoustic wave

Flow Control Laboratory, Department of Mechanical Engineering, KAIST, Daejeon 305-338, Korea. E-mail: hjsung@kaist.ac.kr

† The research works cited in this frontier review have been carefully selected. These articles have not appeared in the recent review papers covering surface acoustic wave microfluidics. The authors report no conflict of interest and are unaware of any biases that might be perceived as affecting the objectivity of this review.

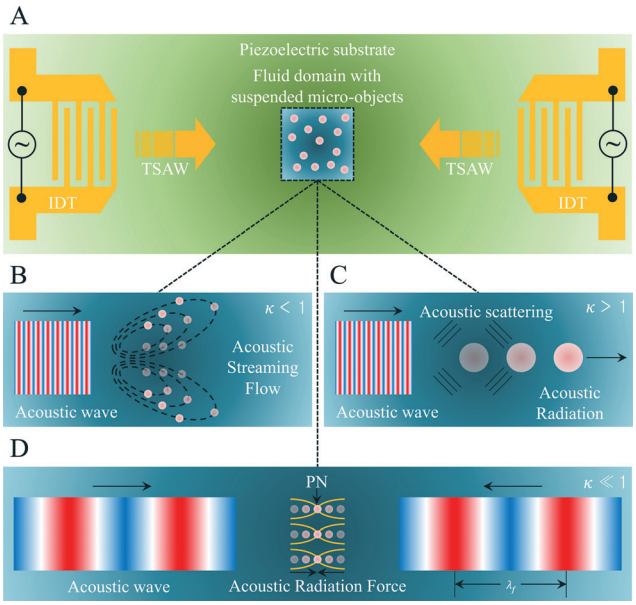

Fig. 1 Schematic representation of micro-object manipulation and microfluidic actuation *via* TSAWs and SSAWs. (A) A SAW-based acoustofluidic device composed of IDTs and a fluid domain carrying the particles. (B) The particles are much smaller than the TSAW wavelength, as $\kappa < 1$, and an acoustic streaming flow (ASF) is produced. (C) A TSAW scattered from the microsphere surface imparts an acoustic radiation force (ARF), as $\kappa > 1$, which dominates the ASF-induced drag force on the particles. (D) Two oppositely propagating acoustic waves interfere to form a standing wave with PNs. The particles drift towards the PNs under the ARF as $\kappa \ll 1$.

frequency and c_f is the speed of sound in the fluid. The dimensionless parameter κ has been extensively used in the field of acoustics as it provides a useful estimation of the physical dimensions (particle diameter here) with respect to the sound wavelength. Moreover, most of the particle-based microfluidic studies employ PS microspheres or microbeads to test their hypotheses. Therefore, it is important to note that the κ values calculated for PS particles in this study may not apply to other particle materials, droplets or cells. A separate analysis would be required to draw respective conclusions. For constant-frequency travelling acoustic waves and PS particles with smaller diameters compared to sound wavelength ($\kappa < 1$), the particles are not influenced by the ARF and are trapped in the ASF vortices (see Fig. 1B); however, the ARF dominates the ASF for particles with larger diameters ($\kappa > 1$), a condition that is useful for manipulating the micro-objects based on their acoustic properties (see Fig. 1C). ASF, on the other hand, is used to induce mixing in the laminar flow on the micro-scale, pump fluids, and even separate particles in a micro-sessile droplet. The boundary value 1 for κ is not absolutely strict, as the above conditions are crude estimations of the two phenomena (ARF and ASF) and hold true only for spherical PS particles suspended in water. Several other factors will come into play for a particular case where a particle with a different material is suspended in a different fluid. ARF is critically dependent on the shape and size of the micro-object, and densities and sound speeds of both the fluid and the particle. ASF is strongly affected by the viscosity and density of the fluid, acoustic attenuation length scale, dimensions of the fluid domain and the frequency of the travelling acoustic wave. Details regarding the κ factor, ASF and ARF can be found in the later sections.

A pair of acoustic waves propagating in opposite directions forms a standing wave with regions of minimum and maximum pressure fluctuations, known as pressure nodes (PNs) and anti-nodes (PAs), respectively (see Fig. 1D). The frequency associated with standing waves is usually low ($\kappa \ll 1$) compared to that of the travelling waves, and even smaller particles can be driven towards or away from PNs, depending on the relative density and compressibility of particles and fluids. Standing waves are useful for focusing, separating, aligning, patterning, and tweezing micro-objects.

Ghulam Destgeer

Ghulam Destgeer received his Bachelor of Science in Mechanical Engineering degree from Ghulam Ishaq Khan (GIK) Institute of Engineering Sciences and Technology, Pakistan in 2010. He worked as a lab engineer at GIK Institute for one year before joining KAIST, Korea as a graduate student in 2011. After obtaining his Masters of Science degree from KAIST in 2013, he is currently in the 2nd year of his pursuit of a PhD degree in Mechanical Engineering. He has been investigating travelling surface acoustic wave-based separation of particles. His research interests include microfluidic lab-on-a-chip technology in general and acoustofluidics in particular.

Hyung Jin Sung

Dr. Hyung Jin Sung is a principal investigator at the Flow Control Laboratory and a professor of Mechanical Engineering at KAIST, Korea. He received his bachelor's degree from Seoul National University and his PhD degree from KAIST. He has been enlisted as a fellow of the American Physical Society (APS) in 2013 for his contributions to turbulence, fluid–structure interaction and opto/microfluidics. He is also a recipient of KAIST Grand Prix Academic Award in 2009. He has been a co-author of more than 250 journal articles. His research interests include acoustofluidics, optofluidics, particle image velocimetry, fluid–structure interactions and turbulence.

Various recent reports of microfluidic actuation and micro-object manipulation are categorized according to the use of TSAWs or SSAWs in Table 1. The TSAWs exhibited tremendous potential in their ability to actuate fluids in various microfluidic operations, such as mixing, translocation/pumping, atomization/nebulization, swimming, counter-flow pumping (flow reversal), and droplet generation and size control.[5–22] Different from SAWs, another type of waves (Lamb waves) produced in the bulk of an LN substrate connected to low-cost metal electrodes was found to produce a novel poloidal flow inside micro-sessile droplets.[23,24] TSAWs may also be used to manipulate (separate, sort, merge, lyse, *etc.*) micro-objects inside a micro-sessile droplet,[25–28] a microchamber,[29] or a microfluidic channel,[30–38] based on ASF-induced drag forces or direct ARF. Recent uses of SSAWs to manipulate micro-objects are also summarized in Table 1. Conventional SSAWs form one or more PNs inside a microchannel, and these PNs may be used to realize microfluidic cytometers, separate bacteria or vesicles, enrich low-abundance cells, or co-culture different cancerous cells in a controlled manner.[39–44] Cell separation and washing may be realized using tilted angle SSAWs (taSSAWs) that form one-dimensional (1D) PNs with multiple nodal lines distributed along a line which is angled with respect to the flow direction.[45–47] Two-dimensional (2D) SSAWs may be used to precisely control cell–cell interactions and induce reparable sonoporation in a cell by bursting a microbubble in its vicinity.[48,49] Tunable patterning of silver nanowires and rapid deagglomeration of carbon nanotubes from a bundle have also been realized.[50,51] SSAWs are usually produced when a pair of parallel IDTs is actuated simultaneously; however, a single IDT has been found to produce standing acoustic waves that proved to be a useful alternative for micro-object manipulation (focusing and sorting).[52–54]

Two comprehensive reviews of SAW-based microfluidics were recently presented, covering an extended list of publications dating back to the start of acoustofluidics.[3,4] The present review differs in that it covers the literature beyond these reviews and provides another perspective on some of the issues that have been only tangentially addressed, such as the characterization of ARF applied to particles *via* TSAWs, the distinction of ASF-induced drag force from ARF, *etc.* Ding *et al.*[4] provided an extensive summary of SAW-based acoustofluidic studies; however, clear theoretical explanations

Table 1 Summary of the literature reviewed here

Mode	Principle	Operation	Remarks	Ref.
Previous literature	Book	Microscale Acoustofluidics	Extensively covers bulk and surface acoustic waves' applications in microfluidics	1
	Reviews	Technical feature	Highlights the importance of sound in moving micro-objects in a contact-less manner	2
		Critical reviews	Covers most significant SAW-based research since the inception of the acoustofluidic field	3, 4
TSAWs	Microfluidic actuation	ASF-based microfluidic actuation inside a micro-sessile droplet and a microfluidic channel	ASF characterization inside a sessile droplet	5, 6
			Gradient generation and mixing inside a microchannel/chamber; translocation of droplets on a substrate surface for splitting and merging	7–10
			ASF-based application using new thin piezoelectric films and different wave modes	11–13
			Nebulization, swimming and pumping	14–17
			Counter-flow pumping and flow reversal in thin liquid films	18–20
			Droplet generation and size control	21, 22
		Lamb waves for microfluidic actuation[a]	Low cost metal electrodes used to realize various acoustofluidic operations including poloidal flow	23, 24
	Micro-object manipulation	ASF-based manipulation of microparticles	Sorting of cells based on their density differences and adhesive properties inside a sessile droplet	25–27
			Lysing of exosomes for RNA extraction and shear-induced cellular uptake of nanoparticles	28, 29
			Fluorescence-activated continuous sorting of cells and droplets inside a microchannel	30
		ARF-based manipulation of microparticles	Continuous sorting, separation or merging of micro-objects inside a microchannel	31–38
SSAWs	Micro-object manipulation	1D SSAW with single or multiple PNs	Particle focusing to realize a cytometer; *E. coli* bacteria separation, microvesical purification, and cell enrichment and co-culture	39–44
		taSSAW with multiple PNs	Cell separation and washing	45–47
		2D SSAW	Precise control over cell–cell interactions and reparable sonoporation of cells	48, 49
		Nanowire and nanotube manipulation by SSAW	Alignment of silver nanowires using the DEP force, and deagglomeration of carbon nanotubes	50, 51
		Single IDT for producing SSAW	Superstrate resonant cavities and PDMS pillars for producing standing acoustic waves	52–54

[a] A non-SAW technique; Lamb waves are produced using a similar LN substrate (as used for SAW devices) and low-cost metal electrodes.

of TSAW-based particle manipulation have been lacking. Theoretical discussion of TSAW-based particle manipulation has been intermixed with discussions of standing acoustic waves. The threshold diameter (the diameter at which the ARF dominates the ASF-induced drag force) of 1.4 μm for a 2 MHz frequency is wrongly attributed to TSAWs, which was originally estimated using standing waves. The threshold diameter can be estimated based on $\kappa = \pi df/c_f \approx 1$, as a TSAW (frequency of 200 MHz) interacts with a PS particle, such that $d \approx 2.5$ μm.[32,35] Previous descriptions of TSAW-based particle manipulation may be improved upon to better our understanding of the phenomenon. The particle size scaling relationship under TSAWs, in particular, has not been fully treated elsewhere and will be discussed here in detail. As pointed out by Yeo and Friend,[3] the principle underlying the formation of SSAWs has also been misunderstood by many; contrasting arguments will be presented later in this paper to highlight the missing explanations to be asked in the future. For a comprehensive literature survey of the acoustofluidic field (which covers bulk as well as surface acoustic waves), readers are referred to a recently published book by the Royal Society of Chemistry entitled "Microscale Acoustofluidics".[1] Vivien Marx emphasised the importance of acoustofluidic manipulation of micro-objects while summarizing the pros and cons of bulk as well as surface acoustic wave-based techniques.[2]

The present article deals with the most recently reported SAW-based studies not covered in recent reviews.[3,4] We have strictly selected articles published in year 2013 and onward. The present article categorizes, discusses, and critically analyses the studies summarized in Table 1. We close with a discussion of possible future developments in the field of acoustofluidics.

Travelling surface acoustic wave microfluidics

In a microfluidic system, TSAW-based ASF and ARF have found several applications. TSAW-based ASF was used to actuate a micro-sessile liquid droplet to enable controlled mixing,[6] pumping,[11] jetting,[12] nebulizing[14] and atomizing of a fluid (see Fig. 2A). Moreover, ASF was employed to generate a concentration gradient inside a microchannel,[7] to propel floating objects,[16] and pump fluid across reservoirs[17] and through microchannels[19] (see Fig. 2B–E). Microscale-thin films drawn from a fluid, known for their inherent complex nature, were recently studied in detail while inducing double flow reversal[20] (see Fig. 2E). To generate droplets in a continuous flow inside a microfluidic channel, an interface between two immiscible fluids with different acoustic impedances was actuated by the TSAW-based ARF (see Fig. 2F).[21] A non-SAW fluid actuation mechanism based on Lamb waves was discussed as a potential alternative to SAWs (see Fig. 3).[24] The ASF produced by TSAWs has found several applications in cell sorting based on density differences[25] and adhesive properties[27] (see Fig. 4A). TSAWs, unlike SSAWs, have long been overlooked for their potential to handle (deflect, separate, sort and trap) micro-objects using the ARF.[31] The scattering of high-frequency travelling acoustic waves from a PS particle having a diameter comparable to the sound wavelength λ_f in the fluid (*i.e.* $\kappa = \pi d/\lambda_f \gtrsim 1$) produces a strong ARF. The separation of particles using a TSAW-based ARF was only recently demonstrated in a continuous flow, after the phenomenon had become better understood (see Fig. 4B–E).[34–36] The ARF was further incorporated to trap and coalesce droplets in a microchannel (see Fig. 4F).[38] In the following subsections, we will discuss various microfluidic actuation and micro-object manipulation techniques developed recently using the ASF and the ARF generated by TSAWs.

Microfluidic actuation

Acoustic streaming flow characterization. TSAWs have performed commendably in microfluidic actuation applications in confined (microchannel/chamber) as well as open spaces (sessile droplets). Fluid actuation is accomplished by the ASF produced as a result of sound energy dissipation inside the fluid when an acoustic wave propagates through it.

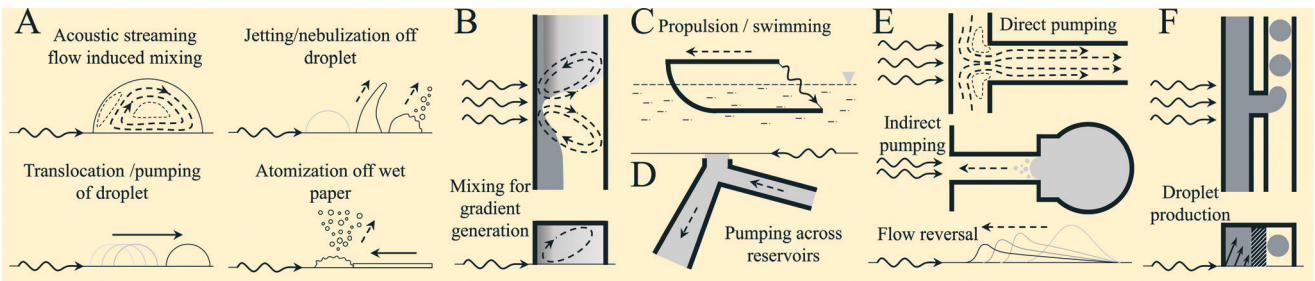

Fig. 2 Microfluidic actuation *via* TSAWs. (A) An acoustic streaming flow (ASF) produced inside a micro-sessile droplet exposed to the TSAWs. Droplet translocation or pumping using a high input power, provided that the surface of the substrate is properly prepared (hydrophobic or oleophobic, depending on the fluid used). Jetting or nebulization off a water droplet trapped in a hydrophilic patch surrounded by a hydrophobic surface at high input powers. Atomization/nebulization realized by continuously drawing fluid through a wet paper or a capillary tube.[6,12] (B) Chemical concentration gradient generation *via* controlled mixing of fluids induced through the ASF.[7] (C) Floating body swimming *via* a TSAW-based propulsion mechanism.[16] (D) Pumping across reservoirs with constantly changing pressures.[17] (E) Acoustofluidic direct and indirect pumping inside a microchannel, and reverse fluid flow induced by high-frequency TSAWs.[18,20] (F) Droplet production by actuating a water–oil interface using focused TSAWs.[21]

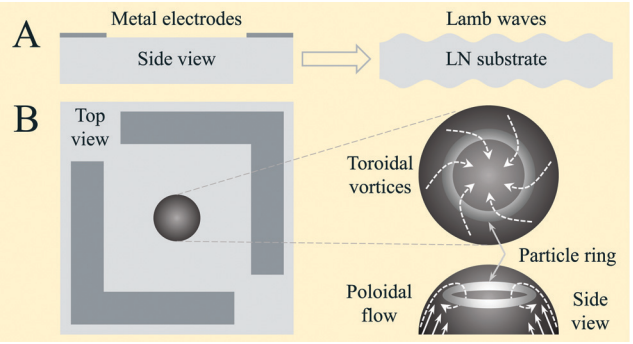

Fig. 3 Novel fluid actuation techniques. (A) A non-SAW acoustofluidic device composed of an LN substrate and low-cost metal electrodes produced Lamb waves when actuated by a resonant frequency AC signal.[23] (B) A poloidal flow, induced by Lamb waves, produced toroidal vortices to form a ring of particles.[24]

As a SAW travelling on the surface of the substrate interacts with a fluid and leaks into it, the wave on the surface and the longitudinal leaky wave in the fluid both decay exponentially, producing a high pressure gradient that results in the ASF. Dentry *et al.*[5] comprehensively characterized the phenomenon while studying the effects of the frequency on the ASF. The model proposed by Dentry *et al.* removed the singularity problem that arose when an acoustic source was modelled using Lighthill's classical model. TSAWs with frequencies ranging from 20 to 936 MHz were tested to characterize the phenomenon for a variety of applications. The experimental setup included a vertically mounted SAW device that was partially immersed in a water-filled chamber. The acoustic beam was found to be attenuated on a length that scaled inversely with the square of the frequency, whereas higher frequencies decayed faster but produced stronger acoustic streaming velocities. The TSAW was attenuated on the substrate surface but also in the fluid, and the attenuation length played an important role in the fluid actuation process. The benefits of utilizing high frequencies beyond 100 MHz were minimal compared to the costs; hence, the actuation frequencies must be chosen carefully with respect to the scale of the required fluid flow and the desired acoustic streaming microfluidic application. For example, an ASF may be induced in a nanolitre droplet using TSAW frequencies up to 1 GHz.[6] The work of Dentry *et al.*[5] is quite comprehensive and detailed, as it covered a broad range of frequencies for ASF production; however, the use of 4.8 μm particles to characterize the phenomenon does not seem suitable, as the ARF acting on the PS particles also becomes significant at higher frequencies (for $f > 100$ MHz, $\kappa > 1$). Although the TSAWs decay fairly quickly at higher frequencies, the effects of the ARF would be present and may contribute along with the ASF to the particle velocity.

Mixing inside a droplet. Fluids in a microliter droplet (with a diameter on the order of millimetres) could be readily mixed as the frequencies required to actuate the fluid were of the order of 10–100 MHz (see Fig. 2A). The difficulties arose in mixing fluids in smaller droplets (nanolitre volumes) due to the formation of standing waves in the droplet that prevented the generation of a strong ASF. Mixing inside nanolitre droplets (diameter $\gtrsim$ 100 μm) using a strong ASF was demonstrated by Shilton *et al.*,[6] who used TSAWs with ultrahigh frequencies (up to 1.1 GHz) such that the acoustic attenuation lengths in the fluid and on the substrate were ~50 μm and ~20 μm, respectively. A droplet with a 1.2 nL volume has a diameter of ~100 μm on the substrate surface, greater than the sound attenuation length scales and much greater than the TSAW wavelength of 3.2 μm (1.1 GHz). Very useful guidelines for characterizing the ASF were provided. The leaky TSAW attenuation length in the fluid droplet was described by the equation $x_f = 3\rho_f c_f^3/16\pi^2\eta f^2$, where ρ_f is the fluid density and η is the fluid dynamic viscosity (mistakenly denoted as the kinematic viscosity by Shilton *et al.*[6]). The attenuation length of the TSAW on the substrate surface was defined as $x_s = 0.45\lambda_s\rho_s c_s/\rho_f c_f$, where λ_s is the wavelength of the TSAW on the substrate surface, c_s is the speed of sound on the substrate surface, ρ_s is the substrate density, and 0.45 is an empirical factor. If $x_f < h$ (height of the droplet),

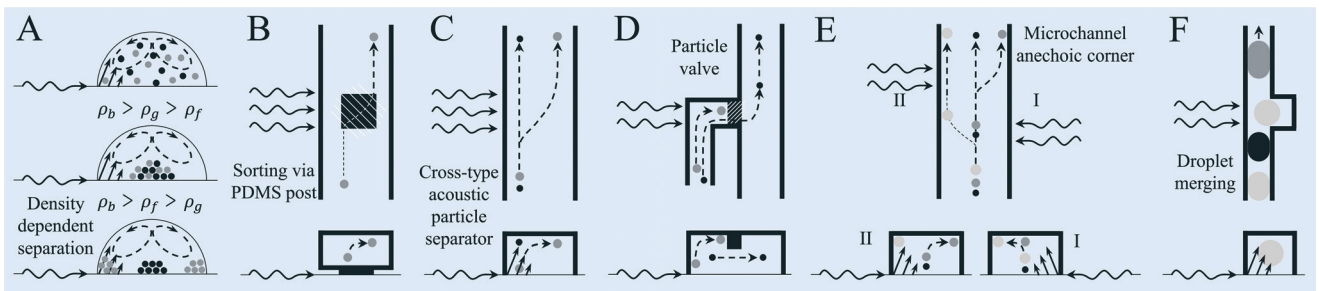

Fig. 4 Micro-object manipulation *via* TSAWs. (A) Microparticle separation inside a micro-sessile droplet, based on density differences, *via* the ASF. All particles were concentrated in the centre of the droplet if the particle densities (black ρ_b and grey ρ_g) exceeded the fluid density (ρ_f) *i.e.* $\rho_b > \rho_g > \rho_f$, whereas separation was realized by adjusting the density of the fluid such that $\rho_b > \rho_f > \rho_g$.[25] (B) A double-layered PDMS microchannel, having a PDMS post underneath, was integrated with the LN substrate to couple the TSAWs from the surface to the microchannel.[30,35] (C) Cross-type acoustic particle separator (CAPS) for continuous particle separation inside a single-layered PDMS microfluidic channel.[31,32] (D) Particle valve for on-demand particle trapping, release, and filtration using a thin PDMS membrane inside a double-layered microfluidic channel.[34] (E) Microchannel anechoic corner for size-selective three-way separation of particles.[36] (F) On-demand droplet merging using a focused IDT and a microchannel with variable width.[38]

compartmentalized three-dimensional (3D) vortices were produced separately in the front and rear parts of the droplet, whereas if $x_f > h$ ($>\lambda_f$), standard dual vortices were created. For most acoustofluidic applications involving a sessile droplet with diameter d_s, the condition ($d_s \gg x_s$) holds true. The ASF vortices are generated easily as the wave on the surface attenuates rapidly, and a large acoustic energy gradient is present inside the droplet. For $d_s > x_s$, the ASF is generated in a similar manner; however, for $d_s < x_s$, standing bulk acoustic waves are produced. For $d_s \ll x_s$, particles accumulate in rings inside the droplet due to the formation of strong standing waves.

The results of Shilton *et al.*[6] could be compared with prior explorations of the κ-factor. The experiments were conducted using frequencies of $\lesssim$1.1 GHz and particles 0.5 μm in diameter, such that the value of $\kappa \lesssim 1.16$. This means that the ARF on the microparticles could have dominated the ASF for the highest frequency (1.1 GHz) only. We argue that the ASF still dominated (as reported by Shilton *et al.*[6] due to $\kappa < 1$ at all other frequencies tested) for the following reasons: the high-frequency TSAWs (1.1 GHz) decayed completely within 50 μm in the fluid and within 20 μm in the substrate; therefore, the ARF acting on the microparticles was only dominant in the frontal region of the droplet. The particles were deflected from the frontal region by the ARF to a length on the order of the attenuation length scale. As the ASF was present throughout the droplet, the ASF dominated in the rear part of the droplet, and the particles moved with the vortices.

Mixing inside a microchannel or chamber. Inside a microfluidic channel (width (w) × height (h): 500 μm × 140 μm), the ASF induced by the TSAWs (133.3 MHz) mixed the buffer and stimulant solutions to generate an adjustable, rapidly switching chemical concentration gradient (see Fig. 2B).[7] For 133.3 MHz TSAWs, x_f of ~3.6 mm $> h$ and x_s of ~160 μm $< w$. Under these conditions, Destgeer *et al.*[7] observed the formation of a strong ASF with symmetrical vortices, as predicted by the framework proposed earlier.[6] Mixing between two fluids was controlled by varying the input power from 0 to 17.9 V_{RMS}. The required power was relatively higher than that used for most SAW devices as 133.3 MHz was not an ideal resonant frequency for device actuation. Some of the power was reflected back from the IDTs resulting in an overall high power requirement, whereas the resonant frequency was later found to be slightly less than 130 MHz. The rapidly switching gradient operated at 0.25 Hz (*i.e.*, the gradient was switched ON and OFF every 2 seconds), higher than previously reported switching speeds (see Destgeer *et al.*[7] and references therein).

ASF-based mixing was further utilized to realize a completely miniaturized system for chemiluminescence detection and anti-coagulant tests.[8,9] A microfluidic chamber cast in PDMS (8 mm in diameter, 2 mm in height, and 100 μL in volume) was used to mix fluids injected through separate inlets and collected at a common outlet to rapidly detect a chemiluminescence reaction in a continuous flow.[8] The TSAWs (f = 20 MHz) were generated using pulsed electric current signals having a 50% duty cycle to enhance mixing, support the reaction, and reduce the detection time. A similar principle was employed to realize TSAW-based mixing in an anti-coagulant assay.[9] The anti-coagulant diagnostic assay was conducted in an acoustofluidic device composed of a PDMS chamber or vessel (3 mm in diameter) attached to a glass slide at the bottom and open at the top. The PDMS vessel was placed directly on top of the IDT operating at a high frequency (140 MHz) to induce mixing. The device was run by a custom-made RF signal generator with two independent output channels.

Droplet-based pumping/translocation/translation and jetting. The actuation of the liquid droplet placed in the path of a TSAW was demonstrated in a variety of applications, such as ASF-based micro-centrifugation, pumping or translocation of a droplet in the direction of wave propagation, and the production of a jet from a droplet at a high input power (see Fig. 2A). Recently, the splitting of a droplet into two smaller droplets of equal volume was demonstrated on a planar microfluidic platform.[10] A pair of focused IDTs was also used to translocate two smaller droplets relative to each other before merging them to form a larger droplet.[10] Fluid actuation was typically carried out on an acoustofluidic platform built on a 500 μm thick solid piezoelectric LN substrate. Piezoelectric LN is best known for its high electro-mechanical coupling coefficients, transparency, and surface smoothness. Certain limitations of LN, such as its brittleness, failure at high powers, and cost, render it unsuitable for a variety of applications, and researchers have searched for alternative thin piezoelectric films composed of zinc oxide (ZnO) or aluminium nitride (AlN) deposited onto various substrates (silicon, glass, or polymers). These thin films were recently used to demonstrate a range of acoustofluidic operations, as mentioned above (see Fig. 2A), and they offer the advantages of low cost, structural flexibility, high sound velocities, and actuation of various wave modes.[11–13] Thin films, however, suffer from chemical instabilities and low electro-mechanical coupling coefficients, and they require relatively very high input powers to realize effects comparable to those induced on an LN substrate. A recent comprehensive study of AlN and ZnO SAW-based acoustofluidic actuation was conducted, and the results were compared to those obtained using an LN-based system.[11,12] A ZnO/Si substrate supporting a deposited IDT was driven at resonant frequencies of 62–275 MHz to induce streaming, pumping, and jetting in a sessile droplet. The device was covered with a hydrophobic layer to facilitate the pumping action and protect the ZnO film (5.5 μm thick) from chemical damage.[11] A driving frequency of 210 MHz induced streaming, pumping, and jetting at input powers of 5, 16, and 37 W, respectively. The required powers were an order of magnitude higher than those required by LN devices.

The ZnO/Si devices operated in the Rayleigh wave mode only, however, the AlN thin film deposited on the Si substrate displayed different wave propagation modes.[12] The Rayleigh wave mode was realized at 80.3 MHz, and a higher frequency-guided wave mode was realized at 157.3 MHz. The AlN thin film on the Si substrate was chemically more stable than the

ZnO/Si system; however, a hydrophobic layer was deposited to assist the acoustofluidic operation. A comparison with the ZnO/Si devices revealed that the AlN/Si devices were advantageous in that they produced higher sound velocities, and possessed better mechanical properties and resistance to humidity, although they suffered from much higher power requirements, more than twice the powers required by ZnO/Si devices. The surface properties critically affected the type of phenomenon induced. A hydrophobic surface facilitated droplet pumping, whereas a hydrophilic island with hydrophobic surroundings facilitated jetting, as this surface could trap the droplet in a targeted place (see Fig. 2A). Recently, a thin film composed of AlScN (with 27% scandium (Sc)) was used to produce SAWs with a coupling coefficient that was 300% of the coefficient measured on the AlN film, making the AlScN film much more efficient than its counterparts (ZnO, AlN, and others).[13] The reported coupling coefficient, which exceeded 2%, was an order of magnitude larger than that obtained from AlN (0.2%) and comparable to that obtained from LN (5%).

Nebulization/atomization. The actuation of a fluid droplet or a reservoir (in the form of a wet paper) using high-frequency vibrations (with a reasonably high surface acceleration of 10^8 m^2 s^{-1}) and high input powers leads to the formation of aerosol droplets (1 μm in diameter) that break away from the main droplet or reservoir surface.[3] This phenomenon, attributed to the presence of a capillary wave on the free surface of the liquid, is called nebulization or atomization. Nebulization has been used to achieve a variety of objectives to date; however, the underlying mechanism is still not well understood, and mechanistic studies are hampered by challenges inherent to the surprisingly complex nature of the process.

Acoustic nebulization was recently utilized to draw out a precise amount of liquid from a wet paper connected to a reservoir.[14] The mist coming off the liquid film was collected in a superhydrophobic receptacle that was later shaken to merge the small droplets on the surface and form a single droplet of a very precise volume. In another application, a drug delivery device used TSAW nebulization of a liquid drawn out of a wet paper connected to a capillary tube filled with the liquid.[15] The powers required to induce a nebulization process are among the highest powers applied to achieve acoustofluidic SAW-based operations. SAW devices, which are designed with the goal of producing a portable hand-held device, are typically unable to drive nebulization due to the limited power that can be delivered through a portable device. This problem may be circumvented using an amplitude modulation technique that enhances the electrical energy converted into fluid energy and activates capillary waves on the liquid surface that drive nebulization.[15] Amplitude modulation at 0.5–40 kHz allows nebulization processes at power inputs of approximately 1.5 W, thereby reducing the power requirements by one-half and enabling a practical portable nebulizer. The nebulizer was used to deliver biomolecules and antibodies in the form of undamaged mist. The high demand for such devices integrated with amplitude modulation functionalities and low power requirements has tempted researchers to further explore this novel mechanism (see Rajapaksa *et al.*[15] and references therein). This quest has led to the design of non-SAW devices using similar hand-held portable electric circuits that can induce different vibrational modes (Lamb waves) on an LN surface connected to low-cost aluminium electrodes to realize nebulization (the details will be discussed later).[23]

Propelled swimming objects. TSAWs are good at coupling surface vibrations to the contacting fluid, thereby inducing a fast ASF. The ASF is an outcome of a body force within the fluid from the vibrations of the substrate surface. Bourquin *et al.*[16] demonstrated the propulsion of a floating body using the ASF-based body force (see Fig. 2C). The body force, which is a function of the wave frequency and amplitude squared, radiated in the fluid at the Rayleigh angle (approximated by Snell's law to be 22° for water coupled with an LN substrate). The LN substrate that produced the TSAW was attached to a floating body such that the direction of the force was parallel to the water free surface. The 3D printed floating body began to swim upon actuation of the attached IDT at a frequency of 11.83 MHz. A simple IDT was replaced with a slanted IDT (f = 9.2–13.3 MHz) to activate a different region of the LN substrate, thereby changing the location of the force with respect to the body. The direction of the swimming body was manoeuvered by modulating the actuation frequency.

Pumping across reservoirs. SAW-based devices had been used to pump liquid inside a microchannel or translocate sessile droplets on the surface of the substrate (see Yeo and Friend[3] and references therein). The pumping of liquid inside a closed-loop microchannel (a racetrack pumping mechanism) was demonstrated previously without the transfer of liquid from one reservoir to another. The study overcame the constant resistance of the closed-loop microchannel but did not work with variable fluidic resistance, as is required in practical microfluidic systems. The development of methods for continuously actuating fluids enabled the transfer of liquid from one reservoir to another, even if the fluid resistance changed unceasingly (see Fig. 2D).[17] The TSAW device used to pump the fluid was made to maximize the acoustic energy transferred into the fluid along the desired direction. The ASF harnessed here was thoroughly understood and modelled (as demonstrated by Dentry *et al.*[5]) to enable the design of a device based on adjustments to the dimensions of the microchamber, with respect to the sound attenuation length scale that produced the maximum output flow rate.[17] The chamber was aligned along the Rayleigh angle, as was done to achieve a swimming floating body (see Fig. 2C).[16] The TSAW-generating LN substrate was reversibly connected to the 3D-printed microchamber to pump liquid from one reservoir to another that enabled the reusability of the components.

Pumping inside the microchannel. The pumping of fluid inside a microchannel could be categorized as direct or indirect pumping, depending on the direction in which the fluid flowed relative to the TSAW propagation direction (see

Fig. 2E). Counter-flow pumping (indirect) inside a microchannel was realized when the TSAWs evaporated or atomized the liquid from the reservoir, and subsequent coalescence of the mini-droplets drew it through the microchannel in a direction opposite to SAW propagation.[18] The counter-flow pumping mechanism was further enhanced by utilizing ultrahigh-frequency TSAWs (up to 754 MHz) to draw or pump fluid through even narrower microchannels (w ~50 μm). Guidelines for the microchannel width and the effective TSAW wavelength needed to realize pumping were provided as follows: $w \geq 10\lambda_s$, which was further updated in the recent publication as $w \geq 7.5\lambda_s$.[19] Travagliati *et al.*[19] performed counter-flow pumping using 96 MHz TSAWs and PS microbeads (d = 0.5, 2, 5, or 10 μm) suspended in water. The pumping of whole blood through the microchannel was demonstrated while the blood cells were manipulated using the ARF obtained from standing acoustic waves formed inside the channel.[19] Counter-flow pumping requires high input powers (*i.e.*, a higher wave amplitude) that produce strong reflections of the acoustic waves at the PDMS walls and within the fluid itself, resulting in the immediate formation of standing waves inside the fluid. The acoustic waves (f = 96 MHz) decayed over a length scale of approximately 230 μm, comparable to the length scale on which acoustic standing waves formed. A similar behaviour was observed using other particles or whole blood cells, however, larger particles (5 and 10 μm) failed to seed the frontal vortices inside a 70 μm high microchannel which can be attributed to the TSAW-based ARF. The ASF was present in all experiments that enabled pumping, whereas the ARF produced by standing acoustic waves formed patterns of micro-objects close to the meniscus only. Here, we have slightly digressed from the heading of this section, as the TSAWs that drive the flow form standing waves which manipulate micro-objects, rendering this article appropriate for this section.

The mechanism underlying the drawing of fluid through a microchannel remains under debate. One group has suggested that counter-flow pumping is only the outcome of liquid evaporation at the frontal meniscus of a reservoir and the subsequent coalescence of small droplets with the meniscus.[18] A distinct explanation (discussed next) was given for this phenomenon, in which various streaming modes (Rayleigh and Eckart streaming) produce a thin liquid film that protrudes away from the droplet, depending on the surface properties and dynamic contact angle between the liquid and the substrate (see Yeo and Friend[3] and references therein).

Double flow reversal. A thin film was reportedly drawn from a liquid droplet against the direction of TSAW propagation, and the phenomenon was characterized recently through a study of double flow reversal in thin films.[20] The flow, driven by a high-frequency (MHz) TSAW, depended strongly on the film thickness (several microns). Rezk *et al.*[20] used silicon oil films instead of water to avoid evaporation of the liquid and maintain a low contact angle (<20°) with the surface, both of which effects aided flow reversal. A liquid film having a thickness greater than the TSAW wavelength in the fluid (73, 44, or 29 μm, corresponding to 19.5, 32.7, or 48.5 MHz) was driven in the direction of the TSAW; however, the flow was reversed when the film thickness decreased below the TSAW wavelength. A further reduction in the film thickness, below the sub-micrometre viscous penetration depth, produced a flow along the TSAW direction once again. Eckart streaming was responsible for generating flow along the TSAW direction, whereas Rayleigh streaming was responsible for generating the counter-flow. The study provided a very vivid description of the flow reversal phenomenon and assisted our understanding of the counter-flow pumping mechanism. Pumping through the microchannel differed slightly from the induction of double flow reversal in a thin film, as the TSAWs also interacted with PDMS in the former case. The TSAWs, which propagated through the microchannel, could induce vibrations in the PDMS walls that might have acted as vibrational sources to draw a thin liquid film along the PDMS wall. Furthermore, the microchannel used to achieve counter-flow pumping had a height much greater than the TSAW wavelength, but the flow could still be drawn along the direction opposite to the TSAW direction of propagation. There appears to be a need for a greater and more detailed understanding of the mechanism. Further investigations of the flow reversal (or counter-flow) phenomenon as a function of surface properties and liquid contact angle may address this riddle.

Droplet production and size control inside a microchannel. Most of the microfluidic techniques used to produce droplets continuously inside a microchannel are limited in their ability to independently control the droplet production rate. TSAW-based on-demand droplet production has been realized to overcome the limitations of traditional methods.[21] The TSAWs produced an ARF at the interface between two fluids (*e.g.* oil and water) with distinct acoustic impedances. The acoustic energy absorbed by the fluid increased the static pressure on one side, which deformed the interface. The deformed interface then formed a droplet in the continuous flow (see Fig. 2F).[21] The pressure fluctuations induced by the TSAWs inside a microfluidic channel were later harnessed by Schmid *et al.*[22] to demonstrate a versatile approach to acoustically modulate the droplet size inside the microfluidic channel by precisely controlling the pressure of the continuous medium. Unlike syringe-driven droplet size control techniques, which have long response times, the electrically triggered system provided precise and rapid control over a wide range of droplet volumes.[22]

Novel fluid actuation techniques. The use of high-frequency SAWs has been proven to be very effective for driving fluids in a variety of applications; however, the production of SAWs tends to require clean room fabrication facilities and, consequently, high costs. Although LN chips with patterned electrodes (IDT) may be re-used, the costs associated with IDT fabrication remain high. Rezk *et al.*[23] circumvented the need for costly clean room fabrication processes for the IDT deposition step and proposed a low-cost non-SAW acoustofluidic platform based on aluminium foil

electrodes that provide nearly all of the conventional SAW-based functionalities (see Fig. 3A). Their device was composed of an LN substrate and metal electrodes cut from a kitchen-grade aluminium foil. The 500 μm thick LN chip, reversibly attached to 50 μm thick aluminium electrodes, vibrated in a Lamb wave mode when actuated by a MHz AC signal produced by a hand-held palm-size electric circuit (see Rajapaksa *et al.*[15] and references therein). The Lamb wave mode (fundamental, 3.5 MHz) was confirmed using a laser Doppler vibrometer. The device was able to induce nebulization from a water droplet, drive and mix fluids inside a paper microfluidic channel, perform mixing inside a microscale sessile droplet, and concentrate particles through micro-centrifugation.[23] The device offered quite flexible operation, as the microelectrode design could be cut from an aluminium foil. The power requirements were similar to those of SAW-driven devices.

The effectiveness of the Lamb waves was further tested in driving a poloidal flow inside a micro-sessile droplet to form a toroidal particle ring (see Fig. 3B).[24] Metal electrodes deposited through a lift-off process were used instead of aluminium foil electrodes, whereas the commonly used expensive chrome–glass mask in the lithography process was replaced with a polyamide tape. High-frequency Lamb waves (f = 157–225 MHz) produced a poloidal flow (similar to the ASF) with toroidal vortices. The conditions delineated by Rezk *et al.*[24] for poloidal flow formation inside the micro-sessile droplet (radius R) were analogous to those reported by Shilton *et al.*[6] These conditions included $x_s < R$ and $x_f < R$. The poloidal flow was traced using 5 μm PS particles. The particles were selected under the assumption that the direct ARF did not affect the movement of particles, in contradiction to the previous observations of others.[32,35] We argue here that the attribution of poloidal flow formation to the ASF was predictable; however, the concentration of 5 μm particles in the toroidal ring could not be explained without considering the effects of the direct ARF on the particles (considering the Lamb waves are travelling waves). According to Destgeer *et al.*[32] and Skowronek *et al.*,[35] the ARF acting on the particles was dominant for $\kappa \gtrsim 1$–1.2; the value of κ was estimated to be 2.35 for f = 225 MHz and a particle diameter of 5 μm. We propose that further investigations using particles with smaller diameter ($\lesssim$2 μm if $f \gtrsim$ 225 MHz) would clear up the mechanism underlying this flow formation, as the ARF effect would be reasonably suppressed.

Micro-object manipulation

The preceding discussion has explored the most recent developments in TSAW-based microfluidic actuation techniques. In addition to these applications, TSAWs have been used to manipulate micro-objects suspended inside a fluid, either using the ASF-induced Stokes drag force or using the direct ARF on the micro-objects. In the following sub-sections, we explore the uses of these two approaches for manipulating micro-objects.

ASF-based handling of micro-objects. Micro-objects were manipulated in both open and closed fluid domains. The ASF generated inside a droplet had been used to mix fluids and concentrate particles using micro-centrifugation techniques. Recently, differences in the cellular densities and surface adhesiveness were used together with a potent ASF to induce the separation of cells for disease diagnostics (see Fig. 4A).[25–27] ASF-based lysing of exosomes and cellular uptake of nanoparticles were also demonstrated.[28,29] Fluorescence-activated sorting of droplets and cells was realized inside a microchannel using ASF-based disruption of the continuous laminar flow of the fluid to deflect micro-objects on demand.[30]

Cell sorting and exosome lysis inside micro-sessile droplets. Recently, Bourquin *et al.*[25] took advantage of the ASF phenomenon to demonstrate a rare-cell enrichment technique for rapid diagnosis. The difference between the densities of micro-objects and fluid were exploited for this application (see Fig. 4A). The relatively low-frequency TSAWs (f ~10 MHz) and appropriately sized microparticles (d ~5 μm) or cells ensured that the ARF did not affect the particle motions, and only the ASF determined the particle sorting effects. The microparticles were separated when the density of the fluid (ρ_f = 1.16 g cm^{-3}) was adjusted relative to the densities of PS (ρ_g = 1.05 g cm^{-3}) and silica particles (ρ_b = 2 g cm^{-3}), such that $\rho_b > \rho_f > \rho_g$. The denser particles (silica) settled at the bottom of the liquid due to gravity, whereas the lighter particles (PS), under the dominant ASF drag and buoyancy forces, moved toward the periphery of the droplet. A less dense liquid (ρ_f = 1 g cm^{-3}) concentrated both types of particles in the centre of the droplet due to the gravitational force and low buoyancy. Similarly, infected red blood cells (iRBCs, 1.077–1.080 g cm^{-3}) and non-infected red blood cells (RBCs, 1.080–1.110 g cm^{-3}) were effectively separated within 3 seconds using an ASF-based device upon suspension in an appropriate liquid solution (1.083 g cm^{-3}). The proposed device could be used for the rapid diagnosis of malaria, sleeping sickness, or other parasitic infectious diseases. The ASF-based drag force was further utilized to detach cells from a substrate based on their adhesive properties for label-free sorting.[26] The adhesive strength could also be characterized for the rapid diagnosis of diseases like malaria.[27] Surface adhesion-based sorting (95% efficiency) of human embryonic kidney cells (HEK 293) from smooth muscle cells (fibroblasts A7r5) has been performed using modulated TSAW signals (17 MHz, 50 ms ON and 150 ms OFF) applied over several cycles of excitation and relaxation.[26] An acoustically actuated sessile droplet (duty cycle of 50 ms) containing cells was deposited onto the substrate surface and then deformed along the direction of the TSAW. The droplet movement left behind a thin liquid tail. The cells were then exposed to cyclic shear stress produced by the ASF that removed them from the surface to realize adhesion-based cell sorting. In a similar manner, malaria-infected RBCs were separated from healthy cells attached to the substrate by selecting them out based on the loose adhesive properties of the latter.[27] The continuous

actuation of a liquid droplet using a 132 MHz TSAW peeled away the loosely bound healthy RBCs, whereas the malaria-infected RBCs remained adherent to the surface. The separation of cells enabled diagnosis of malaria within 60 seconds. In another study, the ASF inside a micro-sessile droplet has been shown to induce exosome lysis within ~30 seconds of device actuation at ~1 W.[28] The TSAWs were used in conjunction with another nano-membrane-based ion-exchange device to detect microRNA for diagnosis of pancreatic cancer. The authors proposed that the observed lysis of exosomes was an outcome of the ARF acting on suspended exosomes. The explanation does not seem plausible as the small size of the exosomes (few micrometres) and low actuation frequency (28.3 MHz) dictate that the ASF should dominate the ARF, providing that there are no standing waves formed inside the droplet. The recent developments in acoustofluidics clearly show that SAWs have tremendous potential to be explored; however, the fundamental understanding of most of the acoustofluidic phenomena is still developing.

Nanoparticle uptake by cells. The ASF has been used to induce strong shear stress on the cells attached to the surface of the substrate to remove them from the surface for characterization of their adhesive properties.[26,27] Strobl *et al.*[29] have recently proposed a focused unidirectional transducer (similar to that of Destgeer *et al.*[7]) to generate a strong ASF without extensively heating the device. The ASF produced by 126 MHz focused TSAWs was characterized using particle image velocimetry (PIV) and PS particles with a reasonable diameter of 3 μm, which affirmed that the ARF on the particles was minimal. The experimental setup was quite similar to that of Dentry *et al.*,[5] where the IDT was hanged vertically in a chamber filled with nanoparticle–fluid suspension and cells adhered at the bottom. The shear rate (~100 s^{-1}) on the cells (endothelial, HMEC-1), produced as a result of the ASF, could increase nanoparticle (platinum-coated CrO_2 particles) uptake. However, a higher shear rate (~2000 s^{-1}) resulted in a significant decrease in the uptake.

Cell and droplet sorting inside a microchannel. Another study reported the sorting of droplets and cells (mouse melanoma cells B16F10) inside a double-layered PDMS microchannel integrated with a fluorescence detection setup to deflect the micro-objects from their trajectories using TSAWs (see Fig. 4B).[30] The fluorescence-activated acoustofluidic sorter was driven by 165 MHz TSAWs operated at several kHz of sorting frequency. The sizes of droplets (~20 μm) that were sorted and the corresponding frequency (165 MHz) suggested that the ARF from the TSAWs may dominate the ASF; however, the authors proposed that the micro-object deflection resulted from the formation of symmetric ASF vortices. The earlier proposed conditions for ARF dominance against ASF will not apply here, even though $\kappa > 1$, as the micro-objects sorted were droplets and cells, not PS particles. The PIV results, obtained using 2 μm PS particles and a 165 MHz frequency (*i.e.* $\kappa \approx 0.7$), indicated that there was no effect of ARF. Moreover, the normalized velocities were shown, which prevented the reader from comparing the ASF velocities to the bulk fluid flow and, therefore, the effectiveness of the ASF against the ARF. The acoustofluidic sorting device has significant potential for future studies, however, further work toward characterizing the effectiveness of the ASF or ARF in this phenomenon would encourage progress in this field.

ARF-based sorting and separation. In addition to effectively actuating microfluidic devices, a TSAW can impose a direct ARF on a micro-object with an appropriate size to perform separation and sorting applications. A single-layered PDMS microfluidic channel was used to separate PS particles of various sizes using TSAWs propagating normal to the fluid flow direction (see Fig. 4C).[31–33] Multi-layer PDMS microchannels have also been employed to filter, trap, sort, and separate micro-objects (see Fig. 4B, D).[34,35] The unique potential of the TSAW microchannel anechoic corner mechanism was explored in an effort to achieve three-way separation of particles and to exchange multiple media (see Fig. 4E).[36] An acoustic band-pass filter for particles is realized to single-out particles of targeted diameter.[37] In addition to imparting an ARF to micro-objects suspended in the fluid, the TSAWs were assimilated with a PDMS microchannel of variable widths to trap and merge droplets on demand (see Fig. 4F).[38] We explore these recent developments below while critically analysing the results.

Cross-type acoustic particle separator (CAPS). We demonstrated a cross-type acoustic particle separator composed of a focused IDT and a PDMS microchannel equipped with an acoustic window to minimize the acoustic energy loss to the PDMS wall (see Fig. 4C).[31] PS particles 3 μm in diameter were separated from particles 10 μm in diameter with a 100% separation efficiency using 133.3 MHz TSAWs. The CAPS device was advantageous in that the microchannel alignment with the IDT was flexible and required single IDT actuation, unlike conventional SSAW systems that required two IDTs tightly aligned with the microchannel. A similar separation mechanism was used to realize the submicron separation of particles having diameter differences of less than one micrometer.[32] PS particles with diameter differences of as low as 200 nm were separated using TSAWs produced at various frequencies (129, 155, 192, and 200 MHz). A theoretical framework was developed to support the separation mechanism. The device fabrication process was simple; however, the PDMS microchannel was irreversibly bonded to the substrate, making reuse of the same LN-chip with other microchannels difficult, as the PDMS could not be easily removed.[31,32]

Microscale anechoic architecture for particle separation. Recently, Behrens *et al.*[33] reported a TSAW-based separation device composed of a microscale anechoic architecture that avoided wave reflections from the microchannel wall, thereby preventing the formation of standing acoustic waves inside the microchannel. The device operated at a relatively low frequency (30 MHz) and separated large particles (25 and 45 μm corresponding to κ-values of 1.57 and 2.83, respectively). A microchannel was incorporated into the device with a

specialized diffuser structure, which was etched in a Si layer and bonded to the LN substrate using UV epoxy bonding. The oxygen plasma bonding process between the PDMS and the LN substrate had not been an efficient method for fabricating microchannels, as the bonding frequently failed, even at higher powers and plasma exposure times of several minutes. The PDMS–LN plasma bond was enhanced by the deposition of a thin layer of SiO_2 on the LN substrate, which also protected the IDTs and substrate surface from mechanical damage.[30,36] A reliable alternative was found in UV epoxy bonding; however, this method required precautionary measures to prevent leakage of epoxy into the main microchannel (see Behrens *et al.*[33] and references therein). It is evident that the irreversibly bonded Si microchannel prevented the reuse of the LN chip, however, the anechoic structure was a useful addition to the acoustofluidic technology for suppressing unwanted standing waves inside a microchannel that could be helpful in realizing novel TSAW-based devices.

Particle valve. Microparticle manipulation has mainly been realized using the lateral deflection of the particles from their streamlines. Not much attention has been directed to the vertical migration of microparticles toward the microchannel ceiling, for the ARF inside the microchannel is directed at the Rayleigh angle (22° relative to the wall, pursuant to Snell's law).[31–33] The vertical component of the ARF inside a microchannel more strongly affects suspended microparticles than the horizontal component. This effect was exploited by Collins *et al.*,[34] who developed a particle valve capable of trapping, releasing, and filtering particles using a thin PDMS membrane fabricated along the ceiling of a microchannel (see Fig. 4D). The larger particles were pushed against the thin membrane trap and the smaller particles flowed past it unaffected. The multi-step fabrication process required to prepare the thin PDMS membrane trap was rather complicated; however, the separation and trapping efficiency of the particle valve was remarkable. The alignment of the IDT with the particle trapping zone was critical here,[34] unlike other separation devices using similar ARF principles.[31–33] The PS particles (2 and 5 μm) were separated using the particle valve and a 132 MHz TSAW that trapped the larger particles against the PDMS membrane (2 μm wide and 29 μm tall), in which the microchannel height was 40 μm. The authors reported that the sorting of PS particles with diameters of 5 and 7 μm was not effective. This behaviour could not be explained using conventional estimates of the ARF, which suggests that the ARF increased with the sixth power of the particle radius.[34] A more compelling estimate of the ARF was proposed by Destgeer *et al.*[32,36] (see references therein), who suggested that the ARF did not always vary linearly against the PS particle diameter or κ-factor but numerous maxima and minima were observed in the plot (ARF factor *vs.* κ-factor) that may explain such a behaviour. PS microparticles of different diameters (5 and 7 μm, corresponding to κ-values of 1.38 and 1.94, respectively) exposed to 132 MHz TSAWs may have received an approximately equivalent value of the ARF that rendered the sorting ineffective. The effects of the particle diameter and the TSAW frequency on the ARF will be discussed later in detail.

Multi-layer microchannels for separation. A bilayer PDMS microchannel with a post (see Fig. 4B) and a slanted IDT, as proposed by Skowronek *et al.*,[35] provides a possible answer to the problem of alignment during fabrication and the need for reuse of the micro-chips. A microchannel was fabricated in two steps: a post was fabricated using a thin PDMS layer, and a channel cavity was patterned separately. These components were then brought into contact after carefully aligning the post with the microchannel to enable permanent bonding. The microchannel assembly was reversibly placed on the LN surface with the help of SU-8 spacers. A similar device was used to sort droplets and cells in an acoustically-actuated fluorescence-activated cell sorter (discussed earlier).[30] The double-layer PDMS microchannel assembly was disposable and did not require tight alignment with the IDT; however, it needed additional fabrication processes and a post-to-microchannel alignment step.[30,35] Skowronek *et al.*[35] provided, a first of its kind, an experimental framework for finding the critical value of the κ-factor. Ranges of frequencies (60–325 MHz) and particle diameters (2–10 μm) were used to establish that the deflection of the particles using the ARF could be realized when $\kappa \gtrsim 1.28$. These findings were later corroborated through a study that reported submicron separation and provided a theoretical framework for the behaviours reported previously.[32]

Microchannel anechoic corner for particle manipulation. The radiation produced by the leaky TSAWs inside the microchannel at the Rayleigh angle was utilized to form an anechoic corner region that harboured particles unaffected by the TSAW-based ARF. The formation of such an ARF-free zone resulting in the particles' indifference to the TSAWs was termed the 'corner effect' and was applied to realize three-way microparticle separation and multi-medium exchange.[36] It was noted that the estimated ARF factor increased with respect to the κ-factor (defined earlier) from a bare minimum (for $\kappa < 1$) to a maximum at $\kappa \approx 1.4$, followed by a series of lows and highs (for $\kappa > 1.4$). The unique behavior observed among PS particles was employed to separate 4.2 μm particles from 3 and 5 μm particles in a single step. The ineffective sorting of 5 and 7 μm polystyrene particles through the particle valve proposed by Collins *et al.*[34] could be understood in terms of these results. The ARF factor estimated at 132 MHz for particle diameters of 5 and 7 μm predicted that the particles experienced similar forces, rendering their separation difficult. A mixture of particles, pumped through the microchannel, was hydrodynamically focused in the centre of the microchannel, as reported by Destgeer *et al.*[36] (see Fig. 4E). A left-propagating TSAW deflected the largest particles into the top-left corner of the microchannel. The particles were further exposed to a right-propagating TSAW downstream of the microchannel, such that the top-left corner acted as an anechoic corner that shielded the largest particles from the TSAW-based ARF. The medium-sized particles were deflected rightward by the right-propagating TSAW. The

three-way separation of particles was realized by tuning the frequency of either the left- or the right-propagating TSAWs with respect to the particle diameter. The three-way separation of 3, 4.2, and 5 μm particles was achieved using 135 (left-propagating) and 175 MHz (right-propagating) TSAWs. The device was further utilized to exchange the medium around 5 μm PS particles.

Band-pass filter for particles. A device, similar to that of Destgeer *et al.*,[36] with laterally displaced IDTs, one on each side of the microchannel has been reported to realize a band-pass particle filter.[37] Skowronek *et al.*[37] pumped a mixture of PS particles (3, 4.5, and 10 μm) through the microchannel as sheath flow pushed the particles against the side wall. A TSAW (165 MHz) deflected the larger particles (4.5 and 10 μm) off their streamlines, whereas the smaller particles (3 μm) remained unaffected. Downstream of the microchannel, a counter-propagating TSAW (83 MHz) deflected 10 μm particles back from the sheath flow into the sample flow. The band-pass filtration of 4.5 μm particles was made possible through harnessing a critical value of $\kappa \gtrsim 1.28$ reported previously by the same group.[35] In a similar manner, two high-frequency TSAWs (330 MHz and 165 MHz) were used to realize the separation of 2 and 3 μm targeted particles from a mixture of 1, 2, 3, and 4.5 μm particles. The TSAW (165 MHz) deflected 4.5 μm particles to a greater extent in comparison with 10 μm particles, whereas an explanation for such a behaviour was missing. The theoretical estimation of the ARF on the PS particles by Destgeer *et al.*[36] suggested that the 4.5 μm particles exposed to 165 MHz TSAWs experienced a stronger force compared to the 10 μm particles. Skowronek *et al.*[37] further provided a band-pass range of 3.7–7.4 μm and 1.7–3.5 μm for mixtures of 3, 4.5, and 10 μm particles and 1, 2, 3, and 4.5 μm particles, as the targeted particles to be filtered were 4.5 μm, and 2 and 3 μm, respectively. In the above summarized studies, the deflection of micro-objects was mainly associated with the ARF produced from the scattering of leaky TSAWs off the microsphere surfaces,[31–37] or from the ASF-induced Stokes drag force.[30] A focused TSAW could also generate a gradient force to trap a droplet before subsequently merging with another droplet for coalescence, as discussed next.[38]

Droplet merging. A passive microfluidic system can continuously merge droplets, but it lacks selectivity. Sesen *et al.*[38] used a focused IDT to selectively trap and merge multiple droplets inside a variable-width microchannel (see Fig. 4F). The focused TSAWs (48.5 MHz) produced a Gaussian acoustic field that induced a gradient ARF on the droplets which pulled them toward the centre of the acoustic beam. A variable-width microchannel reduced the fluid velocity in the broad trapping region of the microchannel as well as the drag force that acted on the particles, thereby facilitating trapping. The trapped droplet interacted with the next droplet and merged to form a larger droplet. The larger droplet, which filled up most of the channel width, experienced a stronger drag force, resulting in escape from the ARF that had trapped the droplet. The ARF was controlled to vary the number of droplets that merged.

Standing surface acoustic wave microfluidics

The formation of a standing surface acoustic wave on a substrate surface as a result of the constructive interference between two counter-propagating travelling surface acoustic waves may be readily understood; however, the exact mechanism behind the formation of a standing wave with PNs and PAs inside a microfluidic channel/chamber after sound waves have interacted with the fluid remains a subject of debate. Ding *et al.*[4] reported that the formation of standing waves inside a fluid is akin to the mechanism by which a SSAW on the surface forms PNs and PAs as a result of interference between two TSAWs. The particles concentrate at the minimum-pressure locations to induce particle alignment, separation, or sorting. Yeo and Friend[3] provided a contrasting view of the phenomenon while arguing that it has been "widely misunderstood". They proposed that within the fluid, the "particles align with and aggregate onto the PNs" of the bulk acoustic waves (BAWs), which differ from the SSAWs present on the substrate surface and their corresponding PNs. The BAWs are formed as "a consequence of the acoustic waves radiating into the fluid from the SSAW (*i.e.*, a leaky SAW), which reflect off the channel or chamber walls in both cases to produce standing waves in the fluid". They highlighted that the reflection of sound waves was even possible at the free surface of the liquid or at the liquid–solid interface. The alignment of particles along the SSAW PNs (as proposed by Ding *et al.*[4]) was explained as a coincidence when the BAW aligns with the SSAW by chance. Yeo and Friend[3] further emphasized that "it is the sound wavelength in the fluid" that is important for the design of microchannels with an appropriate width and number of PNs across their width.

SSAWs have been widely used to align micro-objects in one and two dimensions, focus them for cytometry applications, and control cell–cell interactions. The use of SSAWs to drive fluids is limited, as the ASF developed by oppositely propagating TSAWs cancel one another, and the overall strength of the streaming flow diminishes; however, two IDTs are sometimes simultaneously actuated to produce vertical liquid jets (see Yeo and Friend[3] and references therein). SSAWs have been used mainly for particle manipulation, and we will discuss the recent advances concerning this discipline in the next section.

Micro-object manipulation

Cytometry. The fundamental mechanism underlying particle focusing was utilized to realize an SSAW-based cytometer for particle and cell counting (see Fig. 5A).[39] An SSAW (f = 19 MHz, λ_s = 200 μm) focused the fluorescent particles or fluorescently labelled cells three-dimensionally inside a PDMS microfluidic channel ($w \times h \times l$: 100 μm × 60 μm × 10 mm) without the use of sheath flow. A laser-induced fluorescence (LIF) detection system was integrated with the SSAW-based focusing device to precisely detect and count the

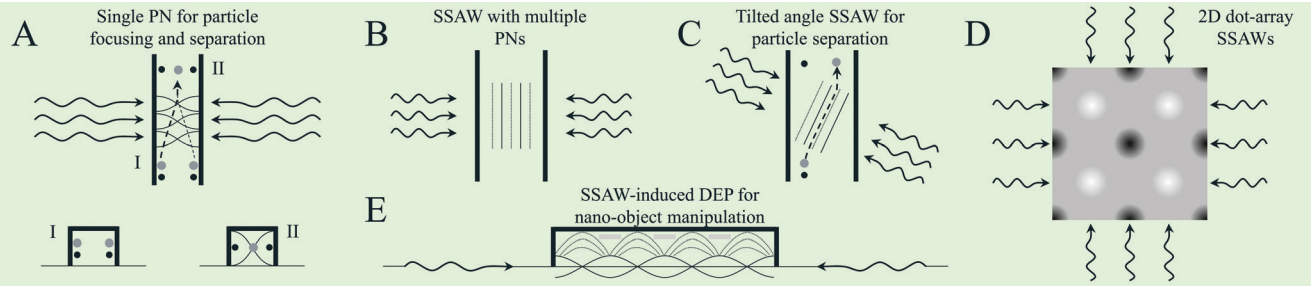

Fig. 5 Micro-object manipulation *via* SSAWs. (A) Conventionally, SSAWs are produced by two counter-propagating TSAWs that interfere constructively and focus the particles or separate them. A cytometer is realized through SSAW-based particle focusing.[39,40] (B) A tunable SSAW capable of producing multiple PNs was used to pattern cells of different types at specific locations to study their interactions.[44] (C) A tilted-angle SSAW device used for micro-object separation and washing.[45,46] (D) 2D SSAWs were produced through the interference of 1D SSAWs aligned normal to each other. Dot array SSAWs are usually used to pattern cells or particles in the form of small micro-islands.[48,49] (E) The presence of a SSAW on the surface of the piezoelectric substrate was associated with an electric field. The SSAW was used to align the particles at the PNs, whereas nanowires were patterned along the electric field lines normal to the SSAW pressure nodal lines.[50]

microparticles or cells at rates as high as 1000 events per second. Fluorescent microparticles 7 and 10 μm in diameter were simultaneously flowed through the microchannel to measure their respective distinguishable fluorescence intensities. Similarly, flow cytometry was performed on fluorescently labelled human promyelocytic leukaemia cells (HL-60). A conventional SSAW-based 3D focusing mechanism with a single PN at the centre of the microchannel has also been used to separate cells or particles of different sizes (see Fig. 5A). The standing acoustic waves were realized using a single IDT and a superstrate microfluidic channel (the details will be discussed later in this section).[52,53]

Separation of *E. coli* bacteria and microvesicles. SSAWs have been used previously to separate micro-objects, mainly using a single PN located at the centre of the microchannel or two PNs located near the side walls of the microchannel. Ai *et al.*[40] proposed the separation of fluorescent particles (green (1.2 μm) and red (5.86 μm)) and biological cells (rod-shaped *E. coli* bacteria 0.5 μm in diameter and 2 μm in length, from peripheral blood mononuclear cells 7.23 μm in diameter) using two PNs formed inside a microchannel ($w \times h$: 120 μm × 25 μm) by SSAWs (~13 MHz, ~300 μm). The authors proposed that the alignment of the microchannel was not critical to the operation of the device using two PNs along the microchannel side walls, unlike the single-PN-based systems that required tight alignment between the microchannels and the IDTs. In a similar device, the separation of nanoscale (<200 nm) vesicles was realized by Lee *et al.*[41] SSAWs (38.5 MHz, 100 μm) were used to separate 190 nm particles from 1000 nm particles inside a microchannel ($w \times h$: 60 μm × 80 μm) for characterization of the device. The separation of exosomes (~100 nm) from microvesicles (~400 nm) was realized, which was the first of its kind for nanoscale separation.

Enrichment of low-abundance cells and macromolecular crystallography. Chen *et al.* proposed an SSAW (19.6 MHz, 200 μm)-based device composed of a disposable micro-tubing channel with numerous PNs aligned normal to the IDTs to capture the targeted particles (7 μm PS particles) or cells (human whole blood) for enrichment.[42] The polyethylene tubing was coupled to the LN substrate using a coupling gel (KY gel) that promoted leakage of the acoustic energy from the substrate surface to the tubing, resulting in the formation of standing waves over a length scale of 5 mm using approximately 50 PNs (or trapping locations). The system provided more than 100-fold enrichment of the sample with a recovery efficiency greater than 90%, along with other advantages, such as parallel processing capabilities realized by installing more tubes on the same chip, simple fabrication requirements, and flexibility in choosing the tubing material. Recently, a similar device was employed to realize macromolecular crystallography.[43] The SSAW (13.4 MHz, 300 μm) microchip, integrated with a glass tube through a coupling gel, could precisely manipulate protein crystals. A 2D SSAW setup was also used to pattern an array of protein crystals.

Cell patterning for co-culture. SSAWs with multiple PNs (lines) inside the microchannel, used previously to pattern particles and cells, were used to pattern and co-culture two different types of cells to enable a study of their heterotypic cell–cell interactions (see Fig. 5B).[44] Epithelial cancer cells (HeLa cell line) were co-cultured with endothelial cells inside a PDMS microchannel ($w \times h \times l$: 1 mm × 100 μm × 12 mm) using SSAWs (~12.78 MHz, ~300 μm) modulated by a phase shift of 180°. HeLa cells injected inside the microchannel aligned along lines with a period of approximately 150 μm, when the SSAW was turned ON. The patterned cells settled down and adhered to the surface when the SSAW was turned OFF. The microchannel was washed to remove free cells, and new media containing suspended endothelial cells were injected into the microchannel. A phase shift of 180° was applied to the SSAWs to pattern the endothelial cells between the adhered HeLa cells. Again, the newly added cells settled down and adhered to the surface, creating an alternate pattern of HeLa and endothelial cells. The cells were co-cultured to study their mutual interactions over a period of 24 h or more. Real-time monitoring revealed a higher mobility among the cancer cells cultured alongside the endothelial cells compared to those cells cultured on their own.

Tilted-angle SSAW for cell separation and washing. An acoustofluidic system based on SSAWs with a single PN plane arranged parallel to the microchannel wall is typically used to separate micro-objects, such that the separation distance is limited by one quarter of the wavelength (see Fig. 5A). Ding *et al.*[45] proposed a tilted-angle SSAW (taSSAW) device that could overcome the limitations of conventional SSAW-based separators by installing IDTs at an angle with respect to the microchannel instead of parallel to the microchannel (see Fig. 5C). The separation distance was increased by a factor of 10 relative to the parallel arrangement. Multiple inclined pressure nodal lines inside the microchannel ensured the separation of particles such that any particles escaping one node were guided along another line downstream. A wide microfluidic channel ($w \times h$: 1000 μm × 75 μm) encompassed multiple nodal lines of the tilted-angle SSAWs (19.4 MHz, 200 μm). PS particles (2 μm from 10 μm, and 7.3 μm from 9.9 μm) and cells (20 μm human breast cancer cells MCF-7 from 12 μm healthy white blood cells) were separated with separation efficiencies exceeding 97% and 71%, respectively. The angle of inclination was determined to reveal that separation was possible at 0–90°; however, the best separation was achieved over the range of 10–15°. Three different particles (4, 10, and 15 μm) were separated, demonstrating a potential application of the device to separation of various components of blood in a single step. The distinguishing characteristic of the taSSAW separation device was the enhanced separation distance, akin to TSAW-based separation of micro-objects.[31,32] The separation of particles with small diameter differences (7.3 and 9.9 μm) was comparable to the submicron separation of particles (3.0 and 3.2 μm) by TSAWs.[32] On this front, SSAWs and TSAWs have shown remarkable progress together, however, TSAWs are yet to be used for ARF-based separation of cells.

A device similar to the taSSAW-based separator was used to wash beads/cells *via* medium exchange inside a microchannel. Li *et al.*[46] demonstrated the highly efficient (97%) washing of 9.77 μm particles from a mixture containing smaller particles (0.87 μm), which were washed away. A sample of lysed blood containing white blood cells was subjected to taSSAWs that washed away WBCs with >97% purity from the debris of the lysed blood. The medium exchange mechanism used here to wash the cells was akin to the TSAW-based dual medium exchange method reported recently.[36] The taSSAW device was further employed to separate circulating tumor cells from a blood sample obtained from a breast cancer patient.[47] A 20-fold higher throughput was reported compared to that of such previously available devices. Separation of several low concentration (~100 cells per mL) cancer cell lines from white blood cells with an 83% recovery rate was demonstrated.

2D SSAW for cell–cell interactions and cell sonoporation. Two-dimensional SSAWs (also known as a net array configuration) were produced when two orthogonal SSAWs with similar frequencies were superimposed. One-dimensional SSAWs are used to focus, sort, or separate micro-objects; two-dimensional SSAWs are used to pattern micro-objects and even manipulate single cells or particles. Two-dimensional SSAWs with a net array configuration were not suitable for precisely controlling cell–cell interactions. Guo *et al.*[48] demonstrated a very refined version of 2D SSAWs that produced a dot array configuration *via* superposition of two orthogonal SSAWs with slightly different frequencies (see Fig. 5D). Unlike the net array configuration of PNs, in which uniformly distributed suspended particles form a net shape when the SSAWs are turned ON, the dot array configuration of PNs produced acoustic wells that attracted the particles or cells towards their centres. The acoustic wells (*i.e.* individual dots in the array) were used to precisely control the positions of two or more cells while efficiently modulating their interactions. The authors first seeded the microchamber with microparticles or cells in an appropriate dilution ratio that regulated the number of micro-objects being controlled by a single acoustic well. A pair of IDTs was activated to first align the particles in straight lines, then the second pair (orthogonal to the first one) was activated to attract the already aligned particles towards one another. It is important to note that the IDT pairs were deposited at an angle 45° to the *X*-direction of the LN substrate to ensure equal resonance frequencies for both pairs of IDTs. The intercellular distances were controlled with micrometre precision, as the gap junction intercellular communication was studied by monitoring the fluorescent dye transfer between cells.

In another study, 2D SSAWs were used to control microbubble positions before destroying them inside a microchamber bearing seeded cells on its surface to realize targeted sonoporation.[49] When the 2D SSAWs were turned ON, several small bubbles moved toward one another and coalesced to form a microbubble that was precisely transported to a nearby cell. A high-power SSAW was then used to destroy or burst the bubble and apply reparable sonoporation to a single cell. The sonoporation efficiency and cell viability were recorded to be 82.4 ± 6.5% and 90 ± 8.7%, respectively.

Nano-object manipulation. The ARF caused by pressure fluctuations in the fluid was usually used to manipulate micro-objects *via* SSAWs; however, an acoustic field present on the surface of the piezoelectric substrate can produce an electric field that can be utilized to manoeuvre micro/nano-objects *via* the accompanying electrophoretic force. Chen *et al.*[50] patterned and aligned silver nanotubes (500 nm in diameter, 50 μm in length) by taking advantage of an SSAW-induced piezoelectric field having a non-uniform charge distribution on the substrate surface, thereby producing virtual electrodes (see Fig. 5E). The nanowires were patterned to form tunable parallel lines and 2D lattice structures with 3D spark shapes *via* 1D and 2D SSAWs, respectively. The nanowires were aligned in the direction of SAW propagation and normal to the acoustic pressure nodal lines. The authors estimated the electrophoretic force to be three orders of magnitude higher than the ARF. A mixture of PS particles and metallic nanowires was subjected to the SSAWs, which revealed that the particles gathered at the PNs, whereas the nanowires were aligned normally between the particles.

In another study, Miansari *et al.*[51] used SSAWs to deagglomerate (break a cluster into single units) carbon nanotubes using a dry and rapid method by taking advantage of the extremely high (10 Mm s^{-2}) mechanical vibrations of the SAW. These vibrations deliver the equivalent effect of striking a bundle of nanotubes 20 million times per second (20 MHz). Recognizing that the separation of carbon nanotubes is cumbersome, even in solution, the present study used a dry setup that highlighted the potential of the SAW technology. The experimental setup was quite similar to that of Guo *et al.*;[48] however, a thin Au layer was deposited directly onto the LN substrate and was grounded purposefully to avoid the electrophoretic force on the nanotubes. Miansari *et al.*[51] argued that the deagglomeration process was entirely regulated by the mechanical vibrations and provided a detailed description of various forces acting on the individual nanotubes, among the nanotubes, and within the nanotube bundle to characterize the phenomenon.

SSAW generation by a single IDT for particle manipulation. SSAWs are typically produced *via* actuation of two IDTs placed parallel to one another; however, a single IDT was used to generate similar effects by producing standing waves inside a microchannel.[52–54] Collins *et al.*[52] demonstrated the separation of microparticles (6.6 μm from 7.0 μm) as well as nanoparticles (300 nm from 500 nm) inside a microfluidic channel bonded directly onto the IDT (see Fig. 6A). The separation was attributed to the DEP force in a microchannel having a low height (15 μm $< \lambda_f =$ 30 μm) and to the ARF in a microchannel having a high height (45 μm $> \lambda_f$). The authors proposed that the IDT disseminated acoustic waves inside the fluid that reflected off the microchannel walls and from within the electrodes to form standing waves inside the microchannel (with the appropriate height). Simulation results revealed that a reasonably strong DEP force close to the electrodes could overcome the ARF. The separation results were encouraging; however, the explanation for the phenomenon was incomplete. The formation of standing waves inside a PDMS channel by single IDT actuation was observed previously by Travagliati *et al.*;[19] however, their description of the phenomenon revolved around acoustic wave reflections from the microchannel walls and ceiling only, even in a microchannel with a height of 14 μm $< \lambda_f \approx$ 15μm. We argue that further investigations of this phenomenon could clarify the existence of the DEP force. For example, a coupling layer between the electrodes and the fluid could be introduced to ensure that the acoustic field alone or the DEP alone was present. There is a possibility of standing wave formation inside the 15 μm high microchannel of Collins *et al.*,[52] considering a similar formation observed in the 14 μm high microchannel of Travagliati *et al.*;[19] even though the frequencies (49 and 96 MHz, respectively) used were quite different, the wavelength of sound in the fluid still exceeds the microchannel height.

A disposable superstrate-based acoustofluidic device was reported by Witte *et al.*[53] to generate standing waves inside a microchannel while running on a single IDT (see Fig. 6B). A disposable superstrate could be disengaged from the microfluidic component and the transducer, offering reuse of the relatively expensive LN chips and the possibility of readily using a different microchannel. This approach was previously suggested to actuate micro-sessile droplets placed on a superstrate for various applications. The Rayleigh waves were coupled with the superstrate (usually glass) through a coupling layer (water or gel). The superstrate vibrated in the Lamb wave mode. Witte *et al.*[53] proposed a multi-layer (glass–SU-8–glass) microchannel as a disposable superstrate that could be actuated by a single IDT to generate standing waves for particle focusing. A slanted IDT (frequency band of 3.5–5.5 MHz) with harmonic responses up to 21 MHz was used to tune the frequency and form a standing wave inside the microchannel ($w \times h$: 173 μm × 35 μm). A single PN was formed inside the microchannel at 4.138 MHz to focus 3 μm particles. The microchannel did not need to be aligned parallel to the IDT, and multiple (two or three) PNs were also produced at higher resonant frequencies (8 and 12.514 MHz). The microchannel structure, which acted as a resonant cavity, provides flexible assembly options and is inexpensive and disposable. Rambach *et al.*[54] reported an acoustofluidic device with parallel IDTs and a bilayer PDMS microchannel (see Fig. 4B and Fig. 6B) that offered most of the advantages discussed above. The SSAWs were produced when both the IDTs were actuated; however, a single IDT could produce a similar effect, as the acoustic waves reflected off the edges of the PDMS post beneath the microchannel constructively interfered to form PNs. A small mismatch in the frequencies (0.15 Hz) of the two IDTs was used to transport the PNs of the SSAW and consequently the beads trapped at the PNs. The proposed device may be used for transportation, separation, and washing of micro-objects.

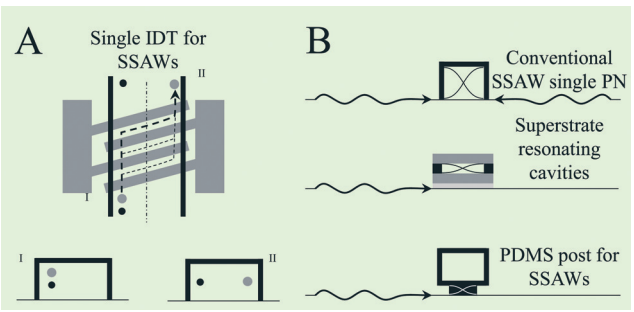

Fig. 6 Single IDT-based SSAW production. (A) A single IDT with a microfluidic channel positioned immediately on top produced standing waves and a variable electric field. The device was used for nano- and micro-particle separation.[52] (B) TSAWs formed from a single IDT can also produce standing waves upon interaction with a superstrate cavity. The reflections of the TSAWs on a PDMS post can also produce SSAWs.[53,54]

Summary and future prospects

This review provides a basic understanding of the different SAW modes, particularly TSAW and SSAW. Starting from an

understanding of the ASF, the attenuation length scales, and the effects of these parameters on mixing and pumping, we moved on to the underlying ARF acting on particles and cells. Various novel approaches have been reported recently in an effort to rapidly expand and apply lab-on-a-chip technologies, including anechoic microchannel and corner effects, tilted-angle SSAWs, and superstrate microchannels. The principles underlying the formation of SSAWs inside microchannels remain a subject of debate, and further studies are needed to improve our understanding of the phenomenon. Acoustofluidic methods are known to manipulate micro-objects suspended in a fluid based on the relative differences in densities, compressibilities, sizes and shapes. The differences in sizes has long been exploited to realize separation, whereas few studies exist that took advantage of the density and compressibility differences. The separation or manipulation of micro-objects of variable shapes or acoustic impedances (density × speed of sound) has yet to be demonstrated. We envision a diaspora of new possibilities emanating from micro-objects of complex shapes. The density and the speed of sound of a material are inter-related properties, hence, instead of considering them separately, we propose to combine the two in a commonly used property of materials *i.e.* acoustic impedance. There has been a lot of progress in the discipline of SAW-based acoustofluidics and a lot more is expected in the coming years as many more researchers have started taking interest in this field.

Acknowledgements

This work was supported by the Creative Research Initiatives (no. 2015-001828) program of the National Research Foundation of Korea (MSIP) and the KUSTAR-KAIST Institute.

Notes and references

1 T. Laurell and A. Lenshof, ed. *Microscale Acoustofluidics*, Royal Society of Chemistry, Cambridge, 2014.
2 V. Marx, *Nat. Methods*, 2014, **12**, 41–44.
3 L. Y. Yeo and J. R. Friend, *Annu. Rev. Fluid Mech.*, 2014, **46**, 379–406.
4 X. Ding, P. Li, S.-C. S. Lin, Z. S. Stratton, N. Nama, F. Guo, D. Slotcavage, X. Mao, J. Shi, F. Costanzo and T. J. Huang, *Lab Chip*, 2013, **13**, 3626–3649.
5 M. B. Dentry, L. Y. Yeo and J. R. Friend, *Phys. Rev. E*, 2014, **89**, 013203.
6 R. J. Shilton, M. Travagliati, F. Beltram and M. Cecchini, *Adv. Mater.*, 2014, **26**, 4941–4946.
7 G. Destgeer, S. Im, B. Hang Ha, J. Ho Jung, M. Ahmad Ansari and H. Jin Sung, *Appl. Phys. Lett.*, 2014, **104**, 023506.
8 A. M. Gracioso Martins, N. R. Glass, S. Harrison, A. R. Rezk, N. A. Porter, P. D. Carpenter, J. Du Plessis, J. R. Friend and L. Y. Yeo, *Anal. Chem.*, 2014, **86**, 10812–10819.
9 S. Meyer Dos Santos, A. Zorn, Z. Guttenberg, B. Picard-Willems, C. Kläffling, K. Nelson, U. Klinkhardt and S. Harder, *Biomicrofluidics*, 2013, **7**, 56502.
10 S. Collignon, J. R. Friend and L. Yeo, *Lab Chip*, 2015, **15**, 1942–1951.
11 Y. J. Guo, H. B. Lv, Y. F. Li, X. L. He, J. Zhou, J. K. Luo, X. T. Zu, A. J. Walton and Y. Q. Fu, *J. Appl. Phys.*, 2014, **116**, 024501.
12 J. Zhou, H. F. Pang, L. Garcia-Gancedo, E. Iborra, M. Clement, M. De Miguel-Ramos, H. Jin, J. K. Luo, S. Smith, S. R. Dong, D. M. Wang and Y. Q. Fu, *Microfluid. Nanofluid.*, 2015, **18**, 537–548.
13 W. Wang, P. M. Mayrhofer, X. He, M. Gillinger, Z. Ye, X. Wang, A. Bittner, U. Schmid and J. K. Luo, *Appl. Phys. Lett.*, 2014, **105**, 133502.
14 T. Vuong, A. Qi, M. Muradoglu, B. H.-P. Cheong, O. W. Liew, C. X. Ang, J. Fu, L. Yeo, J. Friend and T. W. Ng, *Soft Matter*, 2013, **9**, 3631.
15 A. Rajapaksa, A. Qi, L. Y. Yeo, R. Coppel and J. R. Friend, *Lab Chip*, 2014, **14**, 1858–1865.
16 Y. Bourquin and J. M. Cooper, *PLoS One*, 2013, **8**, e42686.
17 M. B. Dentry, J. R. Friend and L. Y. Yeo, *Lab Chip*, 2014, **14**, 750–758.
18 R. J. Shilton, M. Travagliati, F. Beltram and M. Cecchini, *Appl. Phys. Lett.*, 2014, **105**, 074106.
19 M. Travagliati, R. J. Shilton, M. Pagliazzi, I. Tonazzini, F. Beltram and M. Cecchini, *Anal. Chem.*, 2014, **86**, 10633–10638.
20 A. R. Rezk, O. Manor, L. Y. Yeo and J. R. Friend, *Proc. R. Soc. A*, 2014, **470**, 20130765–20130765.
21 D. J. Collins, T. Alan, K. Helmerson and A. Neild, *Lab Chip*, 2013, **13**, 3225–3231.
22 L. Schmid and T. Franke, *Appl. Phys. Lett.*, 2014, **104**, 133501.
23 A. R. Rezk, J. R. Friend and L. Y. Yeo, *Lab Chip*, 2014, **14**, 1802–1805.
24 A. R. Rezk, L. Y. Yeo and J. R. Friend, *Langmuir*, 2014, **30**, 11243–11247.
25 Y. Bourquin, A. Syed, J. Reboud, L. C. Ranford-Cartwright, M. P. Barrett and J. M. Cooper, *Angew. Chem.*, 2014, **126**, 5693–5696.
26 A. Bussonnière, Y. Miron, M. Baudoin, O. Bou Matar, M. Grandbois, P. Charette and A. Renaudin, *Lab Chip*, 2014, **14**, 3556–3563.
27 N. Sivanantha, C. Ma, D. J. Collins, M. Sesen, J. Brenker, R. L. Coppel, A. Neild and T. Alan, *Appl. Phys. Lett.*, 2014, **105**, 103704.
28 D. Taller, K. Richards, Z. Slouka, S. Senapati, R. Hill, D. B. Go and H.-C. Chang, *Lab Chip*, 2015, **15**, 1656–1666.
29 F. G. Strobl, D. Breyer, P. Link, A. A. Torrano, M. F. Schneider and A. Wixforth, *Beilstein J. Nanotechnol.*, 2015, **6**, 414–419.
30 L. Schmid, D. A. Weitz and T. Franke, *Lab Chip*, 2014, **14**, 3710–3718.
31 G. Destgeer, K. H. Lee, J. H. Jung, A. Alazzam and H. J. Sung, *Lab Chip*, 2013, **13**, 4210–4216.
32 G. Destgeer, B. H. Ha, J. H. Jung and H. J. Sung, *Lab Chip*, 2014, **14**, 4665–4672.
33 J. Behrens, S. Langelier, A. R. Rezk, G. Lindner, L. Y. Yeo and J. R. Friend, *Lab Chip*, 2015, **15**, 43–46.

34 D. J. Collins, T. Alan and A. Neild, *Appl. Phys. Lett.*, 2014, **105**, 033509.
35 V. Skowronek, R. W. Rambach, L. Schmid, K. Haase and T. Franke, *Anal. Chem.*, 2013, **85**, 9955–9959.
36 G. Destgeer, B. H. Ha, J. Park, J. H. Jung, A. Alazzam and H. J. Sung, *Anal. Chem.*, 2015, **87**, 4627–4632.
37 V. Skowronek, R. Rambach and T. Franke, *Microfluid. Nanofluid.*, 2015, DOI: 10.1007/s10404-015-1559-3.
38 M. Sesen, T. Alan and A. Neild, *Lab Chip*, 2014, **14**, 3325–3333.
39 Y. Chen, A. A. Nawaz, Y. Zhao, P.-H. Huang, J. P. McCoy, S. J. Levine, L. Wang and T. J. Huang, *Lab Chip*, 2014, **14**, 916–923.
40 Y. Ai, C. K. Sanders and B. L. Marrone, *Anal. Chem.*, 2013, **85**, 9126–9134.
41 K. Lee, H. Shao, R. Weissleder and H. Lee, *ACS Nano*, 2015, **9**, 2321–2327.
42 Y. Chen, S. Li, Y. Gu, P. Li, X. Ding, L. Wang, J. P. McCoy, S. J. Levine and T. J. Huang, *Lab Chip*, 2014, **14**, 924–930.
43 F. Guo, W. Zhou, P. Li, Z. Mao, N. H. Yennawar, J. B. French and T. J. Huang, *Small*, 2015, DOI: 10.1002/smll.201403262.
44 S. Li, F. Guo, Y. Chen, X. Ding, P. Li, L. Wang, C. E. Cameron and T. J. Huang, *Anal. Chem.*, 2014, **86**, 9853–9859.
45 X. Ding, Z. Peng, S.-C. S. Lin, M. Geri, S. Li, P. Li, Y. Chen, M. Dao, S. Suresh and T. J. Huang, *Proc. Natl. Acad. Sci. U. S. A.*, 2014, **111**, 12992–12997.
46 S. Li, X. Ding, Z. Mao, Y. Chen, N. Nama, F. Guo, P. Li, L. Wang, C. E. Cameron and T. J. Huang, *Lab Chip*, 2014, **15**, 331–338.
47 P. Li, Z. Mao, Z. Peng, L. Zhou, Y. Chen, P. Huang and C. I. Truica, *Proc. Natl. Acad. Sci. U. S. A.*, 2015, **112**, 4970–4975.
48 F. Guo, P. Li, J. B. French, Z. Mao, H. Zhao, S. Li, N. Nama, J. R. Fick, S. J. Benkovic and T. J. Huang, *Proc. Natl. Acad. Sci. U. S. A.*, 2015, **112**, 43–48.
49 L. Meng, F. Cai, P. Jiang, Z. Deng, F. Li, L. Niu, Y. Chen, J. Wu and H. Zheng, *Appl. Phys. Lett.*, 2014, **104**, 073701.
50 Y. Chen, X. Ding, S.-C. Steven Lin, S. Yang, P. Huang, N. Nama, Y. Zhao, A. A. Nawaz, F. Guo, W. Wang, Y. Gu, T. E. Mallouk and T. J. Huang, *ACS Nano*, 2013, **7**, 3306–3314.
51 M. Miansari, A. Qi, L. Y. Yeo and J. R. Friend, *Adv. Funct. Mater.*, 2015, **25**, 1014–1023.
52 D. J. Collins, T. Alan and A. Neild, *Lab Chip*, 2014, **14**, 1595–1603.
53 C. Witte, J. Reboud, R. Wilson, J. M. Cooper and S. L. Neale, *Lab Chip*, 2014, **14**, 4277–4283.
54 R. W. Rambach, V. Skowronek and T. Franke, *RSC Adv.*, 2014, **4**, 60534–60542.